Theoretical study of the static screening in insulators: *ab initio* and model dielectric functions

2002 J. Phys.: Condens. Matter 14 4699

(http://iopscience.iop.org/0953-8984/14/18/306)

INSTITUTE OF PHYSICS PUBLISHING JOURNAL OF PHYSICS: CONDENSED MATTER

J. Phys.: Condens. Matter **14** (2002) 4699–4715 PII: S0953-8984(02)30146-2

Theoretical study of the static screening in insulators: *ab initio* and model dielectric functions

Bernard Amadon[1], **Fabio Finocchi**[2] **and Claudine Noguera**[2]

Laboratoire de Physique des Solides, Bâtiment 510, Université Paris-sud, 91405 Orsay cedex, France

Received 26 October 2001, in final form 13 March 2002
Published 26 April 2002
Online at stacks.iop.org/JPhysCM/14/4699

Abstract

We study the screening properties of the three cubic crystals Si, $SrTiO_3$, and MgO, considered as prototypes of materials with various degrees of ionic and covalent bonding. First, we carry out a numerical calculation of the density induced by a short-range time-independent perturbation, in the framework of the density functional theory. The short- and medium-range features of screening are discussed and differences from and similarities with the homogeneous electron gas are stressed. Secondly, we address the question of how local fields can be mimicked by simplified models of the microscopic static dielectric function in which the screening lengths are functions of the unperturbed ground-state local density. While short-range characteristics are fairly well reproduced, we show that the oscillatory behaviour of the induced density in direct space cannot be accounted for by such models. Thirdly, we use the spectral decomposition of the one-electron static polarization response function and propose a simple way to take into account the contribution of the high-energy conduction band states without calculating them explicitly. This method lightens the numerical burden of the polarization calculation considerably and may thus open the way to the computation of static response functions of large systems.

(Some figures in this article are in colour only in the electronic version)

1. Introduction

As screening results from the interaction between electrons and an electric perturbation, it is a general concept encompassing several phenomena in physics. For example, the response of electrons to the creation of extended defects such as surfaces, kinks, etc, or

[1] Present address: CEA, DPTA, Service de Physique de La Matière condensée, BP 12 91680 Bruyèresle Châtel, France.
[2] Present address: Groupe de Physique des Solides, Universités Paris 6-7, Tour 23, 2 place Jussieu, 75251 Paris cedex, France.

point defects and even the band structure, the vibrational properties, and the cohesive energy of solids—constructed from the isolated atoms—may be usefully described in terms of screening. Moreover, many spectroscopic techniques—such as photoemission and inverse photoemission—involve addition or subtraction of electrons, i.e. a modification of the electric field, so the quasi-particle spectra and the optical properties sensitively reflect the screening properties of the system.

Screening was first studied in simple metals [1]; description of screening in insulators is more recent, mainly because of the complexity linked to the strong inhomogeneities of the electronic density. Indeed, the dielectric response in semiconductors and insulators presents two main features which distinguish it from that in simple metals: the screening of a point charge is incomplete—even at a long distance—and strongly anisotropic. This means that the microscopic dielectric matrix in the wavevector space is non-diagonal and the limit of the macroscopic dielectric function for small wavevectors is finite. The former characteristic, the so-called local field (LF) effect, deeply influences the screening characteristics [2]. In real space, they can be described by means of the local electron transfers [3] or, more formally, by the fact that the static dielectric function $\epsilon(\boldsymbol{r}, \boldsymbol{r}')$ is a function not only of $|\boldsymbol{r} - \boldsymbol{r}'|$, as in the homogeneous electron gas (HEG), but independently of the two vectors $\boldsymbol{r}$ and $\boldsymbol{r}'$.

The computation of the *ab initio* dielectric function is a very difficult task even in the random phase approximation (RPA) [2]. The simulation of optical properties in solids using dielectric functions that are calculated from first principles [4, 5] is numerically onerous. A simplified scheme of calculation of the static polarization which avoids the explicit sum over the empty states [6] is expected to open the way to the study of systems containing many inequivalent atoms. An alternative approach may be the use of simplified models of screening which make the computation of the response of the system not much more difficult than the determination of the ground-state properties [7–9]. Based on the seminal paper by Penn [10], several model dielectric functions have been built [11, 12], which include LF effects through the use of the *local density* as the basic variable [13]. Their validity has been checked for semiconductors such as Si, GaAs, GaN [14], but rarely in ionic compounds [15]. The study of the electronic response of iono-covalent materials should permit us to have a better understanding of screening in insulators and to test those approximate models.

The present work aims at achieving some elements of understanding of the following three aspects of static screening in insulators. Firstly, we calculate the induced density in response to a localized static perturbation, in real space, by means of a self-consistent ground-state calculation, in the framework of the density functional theory (DFT). We consider three cubic crystals, namely Si, $SrTiO_3$, and MgO, which span a wide range of ionicity strengths and optical dielectric constants. We extract the main physical effects that reflect the characteristics of screening in semiconductors and insulators. The method of calculation is described in section 2 and the results are presented and discussed in section 3. They are used in section 4 to test the validity of some model dielectric functions [9, 11], for one of which we suggest a simple improvement. Thirdly, in section 5 we propose a simplified method for performing the *ab initio* computation of the static polarizability, which reproduces satisfactorily the behaviour of the induced density, at a low computation cost.

2. Method

2.1. Response functions: basic definitions

We consider the response of the electron gas to the application of a weak static electrostatic perturbation, V_{pert}, in the framework of the linear response theory. In the following, $V_{\text{H}}(n)$

and $V_{xc}(n)$ are the DFT Hartree and exchange–correlation potentials for the density n, respectively. $K_{xc}^{(LDA)}$ is the second functional derivative of the exchange and correlation energy with respect to the density in the local density approximation (LDA), v is the bare Coulomb potential, and V_{e-i} is the interaction between electrons and ions. $n^{(x)}$ and n_0 are the ground-state densities of the solid under consideration with and without a given perturbation potential V_{pert}. (x) stands for the level of approximation at which the electron–electron interaction is taken into account. The induced density $n_{ind}^{(x)}$ is defined by $n^{(x)} - n_0$.

The induced potential $V_{ind}^{(x)}$ is linked to the induced density $n^{(x)}$ and to the response function $R^{(x)}$ by[3]:

$$n_{ind}^{(x)} = \chi_0[V_{ind}^{(x)} + V_{pert}]; \qquad n_{ind}^{(x)} = R^{(x)} V_{pert} \tag{2.1}$$

where χ_0 is the independent particle polarizability. We can compute [2]:

- the induced density in a system of non-interacting electrons (x = NSC):

$$V_{ind}^{(NSC)} = 0; \qquad R^{(NSC)} = \chi_0; \tag{2.2}$$

- the induced density in a system in which the electrons interact only through the Hartree potential during the screening process (x = RPA [16]): the total potential experienced by the electrons is then $V_{e-i} + V_H(n) + V_{xc}(n_0) + V_{pert}$:

$$V_{ind}^{(RPA)} = V_H(n) - V_H(n_0); \qquad R^{(RPA)} = [1 - \chi_0 v]^{-1}\chi_0; \tag{2.3}$$

- the induced density of the interacting system within the LDA (x = LDA). The total potential experienced by the electrons is thus $V_{e-i} + V_H(n) + V_{xc}(n) + V_{pert}$. In this case,

$$\begin{aligned} V_{ind}^{(LDA)} &= V_H(n) + V_{xc}(n) - V_H(n_0) - V_{xc}(n_0); \\ R^{(LDA)} &= [1 - \chi_0(v + K_{xc}^{(LDA)})]^{-1}\chi_0. \end{aligned} \tag{2.4}$$

In each case, it is in principle possible to compute the induced density either by calculating the difference of the ground-state densities with and without the perturbation potential V_{pert} or from the knowledge of the *ab initio* or model response functions. We use these three approaches, depending on what is convenient in the actual case considered.

2.2. Computational details

We choose a Gaussian-type perturbing potential with the same periodicity as the simulation cell ($\boldsymbol{R}_L$ are the lattice vectors). Apart from a constant, V_{pert} reads

$$V_{pert}(\boldsymbol{r}) = -\sum_L A e^{-\gamma(\boldsymbol{r}-\boldsymbol{R}_L)^2}. \tag{2.5}$$

It is created by a charge density that is globally neutral and is consistent with the implicit assumption that the total number of electrons in each simulation cell is a constant. Although qualitatively different from the more realistic Coulomb potential, V_{pert} is sufficient for studying the short- and medium-range responses in real space, which is the aim of the present paper. In the following, we choose $A = 0.03$ Hartree and $\gamma = 1$ au^{-2}. We checked that A is sufficiently small for the induced density to be a linear function of the potential within 0.5%. With a positive value for A, V_{pert} is repulsive for the electrons. The choice of γ is such that the superposition of potentials between two neighbouring cells is negligible.

The density functional calculations are carried out within the LDA for the exchange and correlation [17, 18]. The Kohn–Sham orbitals are expanded in a plane-wave basis set up to a cut-off energy E_{cut}, and separable soft norm-conserving pseudopotentials [21] are used. For

[3] We adopt a matrix notation for the integration over $\boldsymbol{r}$; n and V_{pert} are vectors and χ_0 is a matrix.

MgO and $SrTiO_3$, we adopt the same pseudopotentials as in [15]. For silicon, the core radii in atomic units were chosen as: 1.50 (s), 1.75 (p), 1.75 (d). $E_{\rm cut}$ needed to obtain a convergence better than 3% on the induced density is found to be equal to 30 Ryd for Si, 50 Ryd for MgO, and 60 Ryd for $SrTiO_3$. Except when explicitly mentioned, the simulation cell coincides with the primitive unit cell of the crystal. We used, for Si, MgO, and $SrTiO_3$, 32, 32, and 64 k-points to sample the Brillouin zone, respectively.

We compute the induced density $n_{\rm ind}^{(\rm x)}$ (x = NSC, RPA, LDA) as follows. $n_{\rm ind}^{(\rm LDA)}$ is the difference of the fully self-consistent DFT-LDA ground-state densities $n^{(\rm LDA)}$ and n_0, with and without the perturbation $V_{\rm pert}$, respectively. As far as $n_{\rm ind}^{(\rm NSC)}$ is concerned, we compute the density and the Kohn–Sham potential $V_{\rm KS}(n_0)$ for the unperturbed ground state. Then, we perform a second calculation in which we impose the Kohn–Sham potential to be $V_{\rm KS}(n_0)+V_{\rm pert}$. The difference in the ground-state densities $[n^{(\rm NSC)} - n_0]$ therefore gives $n_{\rm ind}^{(\rm NSC)}$. This induced density, which also reads $\chi_0 V_{\rm pert}$, is used in the following (see section 5) to evaluate the precision of our scheme of calculation of the one-electron *ab initio* polarizability χ_0. In order to compute $n_{\rm ind}^{(\rm RPA)}$, we force the Kohn–Sham potential $V_{\rm KS}(n)$ to be $V_{\rm e-i} + V_{\rm H}(n) + V_{\rm xc}(n_0) + V_{\rm pert}$ at each step of the self-consistent procedure, which yields $n = n^{(\rm RPA)}$. Thus, $n_{\rm ind}^{(\rm RPA)}$ is obtained as the difference $n^{(\rm RPA)} - n_0$. The computed induced potential $V_{\rm H}(n_{\rm ind}^{(\rm RPA)})$ is used in the following (see section 4) to estimate the reliability of RPA model dielectric functions. For the sake of conciseness, such a calculation of the induced densities or potentials is referred to in the following as a *direct method*.

For the purpose of estimating the respective qualities of various approaches as far as the calculation of the static screening of insulators is concerned, the response computed within the direct method is considered as the natural reference. In order to quantify the quality of a given approach (y) for calculating a physical observable $B(\boldsymbol{r})$ such as the induced density or potential, with respect to the direct method, we define a quality coefficient Θ_B given by

$$\Theta_B^{(\rm y)} = \sqrt{\frac{\int {\rm d}^3\boldsymbol{r}\,[B^{(\rm y)}(\boldsymbol{r}) - B^{(\rm direct)}(\boldsymbol{r})]^2}{\int {\rm d}^3\boldsymbol{r}\,[B^{(\rm y)}(\boldsymbol{r})]^2}}. \tag{2.6}$$

The factor $\Theta_B^{(\rm y)}$ is equal to zero if the methods (y) and (direct) yield the same value of B over all space.

In the pseudopotential approach, the core electron contribution to screening is missing, and the electron density does not have the correct node structure close to the nuclei. Nevertheless, it has been successfully used to compute the electronic response [19] and the phonon spectra of many systems [20], in spite of the approximations that have just been mentioned. We also choose to work in such a framework in order to understand the qualitative screening features of the valence electrons in Si, $SrTiO_3$, and MgO (section 3). Moreover, in sections 4 and 5, we discuss simplified approaches to the calculation of the induced density and potentials, which are then compared to the direct method. Actually, the latter calculations are carried out within the pseudopotential approach, but the validity of those simplified methods, and particularly their discrepancies with respect to the direct method, is expected not to depend sensitively on the particular approximation used for calculating the ground-state properties.

3. The induced density in real space

In this section, we report and discuss the spatial dependence of the induced density and potential computed through the direct method in order to extract the main characteristics of the response. Indeed, screening in insulators is less well known than in most metals. In particular, its main features in the HEG, namely the Thomas–Fermi screening length, and the Friedel oscillations,

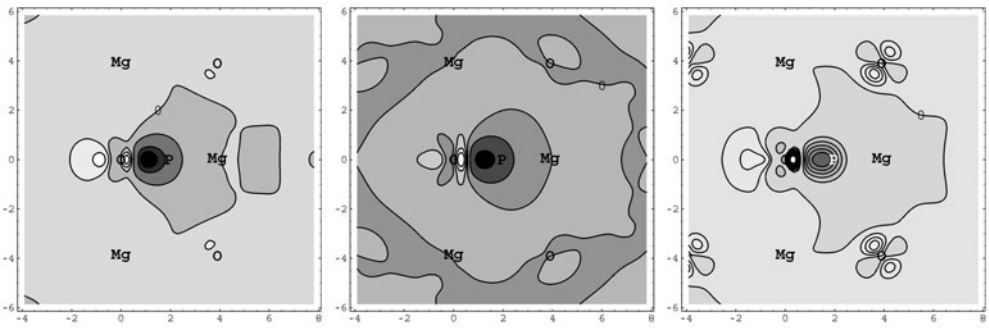

Figure 1. From left to the right, $n_{\rm ind}^{\rm (NSC)}$, $n_{\rm ind}^{\rm (LDA)}$, both in response to a Gaussian potential, and $n_{\rm ind}^{\rm (LDA)}$ induced by a Coulomb potential, in MgO. The perturbation is centred on P, midway between the Mg and the O ions. The dark and bright areas represent negative and positive induced densities. Positive iso-density curves are separated by 0.0002 au^{-3} and negative ones by 0.0005 au^{-3}. Length scales are in atomic units.

cannot be straightforwardly generalized to heterogeneous solids. Finding well-established counterparts of such phenomena in insulators is thus a fundamental issue, which is also relevant to carrying out simplified yet reliable computational schemes for the microscopic dielectric function. To this end, we emphasize the importance of the LF effect: in a truly homogeneous system, the induced density is independent of the point on which the perturbation is centred and isotropic around it, which is not the case in real crystals.

3.1. Range of the perturbation and self-consistent effects

Regarding the specific form of $V_{\rm pert}$, we first check that the main characteristics of the induced density are qualitatively similar when using Coulomb or Gaussian potentials (equation (2.5)). The latter is more suitable from the computational point of view, being of finite range. Indeed, we find that the computed induced density for silicon is qualitatively similar to that obtained by Hybertsen and Louie [22] and Resta and Baldereschi [23] in response to a unique or periodic point charge potentials, respectively. Moreover, as shown in figure 1 (middle and right panels), we find the gross features of the induced densities in MgO—that is, the oscillating behaviour and the spatial extension of $n_{\rm ind}^{\rm LDA}$ around the perturbation site—are similar for both types of $V_{\rm pert}$.

In the left and middle panels of figure 1, one can also get a first insight into the effect of self-consistency on the induced density, by comparing $n_{\rm ind}^{\rm (NSC)}$ and $n_{\rm ind}^{\rm (LDA)}$. They have been obtained for the same Gaussian perturbation, centred halfway between the O and the Mg ions. More precisely, $n_{\rm ind}^{\rm (NSC)}$ and $n_{\rm ind}^{\rm (LDA)}$ are plotted in figure 2 along the Mg–O bond, for two different locations of $V_{\rm pert}$.

$n_{\rm ind}^{\rm (NSC)}$ and $n_{\rm ind}^{\rm (LDA)}$ mainly differ in the vicinity of the oxygen. According to equations (2.1) and (2.4), $n^{\rm (LDA)}$ reads

$$n_{\rm ind}^{\rm (LDA)}(\boldsymbol{r}) = 4 \sum_{i\in{\rm VB}} \sum_{j\in{\rm CB}} \frac{\langle \phi_j(\boldsymbol{r}_0)|V_{\rm pert}(\boldsymbol{r}_0) + V_{\rm ind}^{\rm (LDA)}(\boldsymbol{r}_0)|\phi_i(\boldsymbol{r}_0)\rangle}{\epsilon_i - \epsilon_j} \phi_j(\boldsymbol{r})\phi_i^*(\boldsymbol{r}) \tag{3.1}$$

while $n_{\rm ind}^{\rm (NSC)}$ obeys a similar expression with only $V_{\rm pert}(\boldsymbol{r}_0)$ in the matrix element. Since the induced potential usually counteracts the perturbation, $V_{\rm pert} + V_{\rm ind}^{\rm (LDA)}$ is generally weaker than $V_{\rm pert}$. Such an effect is particularly appreciable in regions where the electron density is high and the Hartree and exchange–correlation components of $V_{\rm ind}^{\rm (LDA)}$ are accordingly large. However,

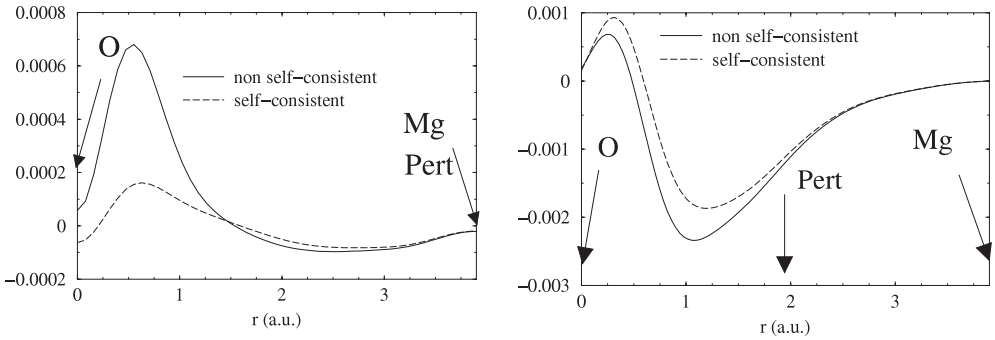

Figure 2. Self-consistent ($n_{\rm ind}^{\rm (LDA)}$) and non-self-consistent ($n_{\rm ind}^{\rm (NSC)}$) densities, in au^{-3}, that are induced in response to a periodic Gaussian potential centred on Mg (on the left) and halfway between O and Mg (on the right) in MgO. The perturbation centre is marked by an arrow labelled 'Pert'.

also in this case, the spatial behaviours of $n_{\rm ind}^{\rm (NSC)}$ and $n_{\rm ind}^{\rm (LDA)}$ are *qualitatively* similar. In the remainder of this section, we mainly discuss the characteristics of the self-consistent $n_{\rm ind}^{\rm (LDA)}$ obtained in our calculations.

3.2. On-site response

In order to identify clearly the short- and medium-range contributions, we calculate the induced density in response to a periodic Gaussian potential by using big enough supercells, containing 8, 16, and 10 atoms for Si, MgO, and $SrTiO_3$, respectively. The corresponding Brillouin zones are sampled at 32, 16, and 56 points. Figures 1, 3, and 4 show some representative plots of the induced density.

The three compounds display some common screening characteristics. Firstly, the induced density depends on the location of the perturbation as a manifestation of LF effects. Secondly, due to the repulsion exerted by the perturbation on the electrons, $n_{\rm ind}(\boldsymbol{r})$ in figures 1, 3, and 4 always has the same sign as $V_{\rm pert}$ close to the perturbation site. The maximum of $|n_{\rm ind}|$ is shifted towards regions of higher total density, whenever the density gradient is large. Thirdly, around the perturbation centre, the larger the ground-state unperturbed density $n_0(\boldsymbol{r})$, the larger $|n_{\rm ind}(\boldsymbol{r})|$.

The expression (3.1) can be used to interpret these results. Indeed, the induced density close to the centre of the perturbation $\boldsymbol{r}_0$ is weighted by the matrix element $\langle\phi_j(\boldsymbol{r}_0)|V_{\rm pert}(\boldsymbol{r}_0)|\phi_i(\boldsymbol{r}_0)\rangle$, which is large when the valence band (VB) state i and the conduction band (CB) state j show some degree of localization around the perturbation. As a consequence, $n_{\rm ind}(\boldsymbol{r}_0)$ is stronger in absolute value when $V_{\rm pert}$ is located close to a region of high density, which is especially the case for oxygen. This qualitatively explains why the model dielectric functions that mimic the LF effects through a functional dependency on $n_0(\boldsymbol{r})$ can give a reasonable description of the induced potential close to the perturbation site. Nevertheless, the perturbation centre does not necessarily coincide with the location of the maximum of $|n_{\rm ind}(\boldsymbol{r})|$, which is displaced towards the region(s) of high electron density.

3.3. Medium-range effects

Apart from the characteristic of the on-site response, one can see in figures 1, 3, and 4, that $n_{\rm ind}(\boldsymbol{r})$ oscillates in the vicinity of the O atoms. A similar effect, although smaller in magnitude,

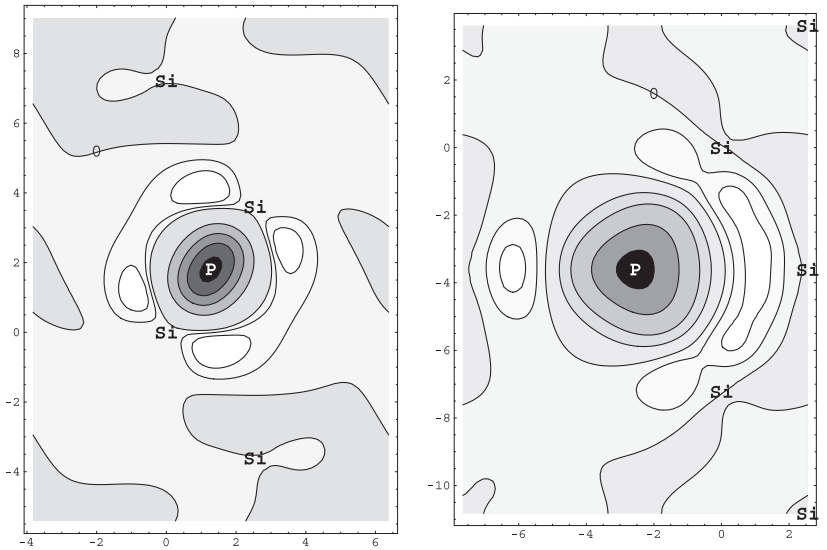

Figure 3. An iso-density map of the induced density $n_{\mathrm{ind}}^{(\mathrm{LDA})}$ in silicon, in response to a Gaussian perturbation localized between two silicons (on the left) and on an interstitial site (on the right). The perturbation is centred on P. The dark and bright areas represent negative and positive induced densities. The iso-density curves are separated by 0.0005 au^{-3} for the negative value and by 0.000 05 au^{-3} for the positive ones on the left. On the right, they are separated by 0.000 04 au^{-3} for the negative value and by 0.000 01 au^{-3} for the positive ones. Length scales are in au.

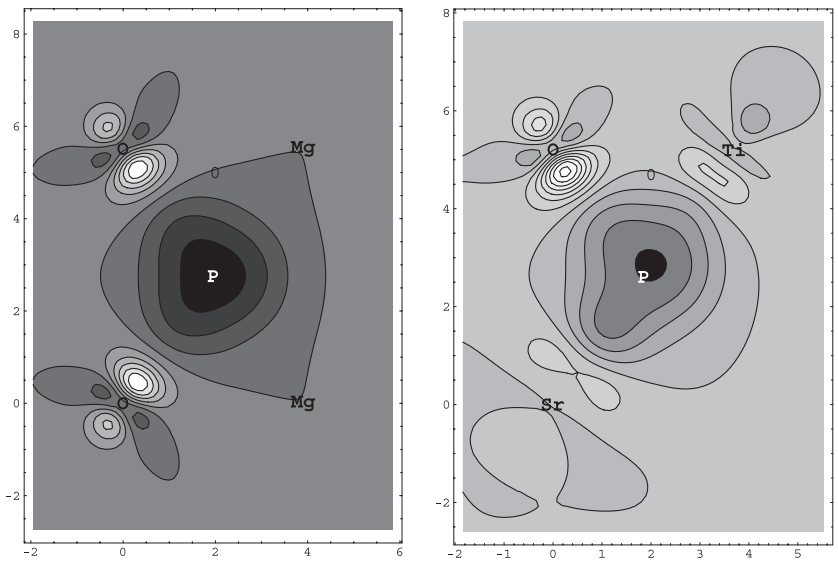

Figure 4. An iso-density map of the induced density $n_{\mathrm{ind}}^{(\mathrm{LDA})}$ in response to a Gaussian perturbation centred on an interstitial site in MgO (left plot) and halfway between Sr and Ti in $SrTiO_3$ (right plot). The perturbation is centred on P. The dark and bright areas represent negative and positive induced densities. The iso-density curves are separated by 0.0001 au^{-3}. Length scales are in au.

may be seen close to the Sr and Ti atoms. In silicon, they are also present (figure 3) but their amplitude is much weaker: the maximum of the positive part of $n_{\mathrm{ind}}(\boldsymbol{r})$ is an order of magnitude smaller than the absolute value of its negative counterpart, while in MgO and $SrTiO_3$ the two extrema have nearly equal intensities. These effects also exist in response to a point charge neutralized by a uniform background (figure 1, right panel) and have also been observed by Hybertsen and Louie [22]. They are thus a genuine physical characteristic of the screening in insulators, independently of the actual shape of V_{pert}.

The shape of the oscillations recalls that of atomic orbitals. Indeed, the oscillations of $n_{\mathrm{ind}}(\boldsymbol{r})$ result from the phase difference between the VB and the CB wavefunctions that appear as a product in equation (3.1). Around the Fermi level, and especially in a very ionic compound such as MgO, the VB states are anion-like and the CB ones are cation-like, and give a large contribution to $n_{\mathrm{ind}}(\boldsymbol{r})$ because the energy difference $(\epsilon_i - \epsilon_j)$ in the denominator is small. In the HEG, in contrast, the PW eigenstates are completely delocalized and contribute to the sum in equation (3.1) giving rise to characteristic oscillations in $n_{\mathrm{ind}}(\boldsymbol{r})$ known as Friedel oscillations. Silicon is a somewhat intermediate case between the latter two systems. We do not discuss long-range effects, whose study is beyond the capability of our calculations, as already pointed out.

4. Model dielectric functions

In this section, we analyse the validity of some simplified models of microscopic dielectric functions built to describe the screening in semiconductors and insulators. In such materials, whereas the finite value of the optical dielectric constant ϵ_∞ can easily be taken into account, it remains a challenge to describe accurately the existence of LF effects. To our knowledge, two RPA models attempt to include LF effects, namely the Levine–Louie (LL) [11] and the Cappellini–Del Sole–Reining–Bechstedt (CDRB) [12] models, which are detailed in the following. As a first step, we compare the induced potential $V_{\mathrm{ind}}^{\mathrm{M}}$ given by model M (M = LL or CDRB) with that obtained by the RPA direct method in DFT-LDA. Then, we propose an improved version of the CDRB model that is based on the same treatment of LF effects. Furthermore, we interpret the results and analyse the limits of such models.

4.1. Theoretical background

The independent electron polarizability χ_0 is related to the RPA dielectric function through the relation

$$\epsilon_{(\mathrm{RPA})}(\boldsymbol{r}, \boldsymbol{r}') = \delta(\boldsymbol{r} - \boldsymbol{r}') - \int \mathrm{d}\boldsymbol{r}''\, v(\boldsymbol{r} - \boldsymbol{r}'')\chi_0(\boldsymbol{r}'', \boldsymbol{r}'). \tag{4.1}$$

The screened interaction $W(\boldsymbol{r}, \boldsymbol{r}')$ can be derived from the knowledge of $\epsilon_{(\mathrm{RPA})}(\boldsymbol{r}, \boldsymbol{r}')$:

$$W(\boldsymbol{r}, \boldsymbol{r}') = \int \mathrm{d}\boldsymbol{r}''\, v(\boldsymbol{r} - \boldsymbol{r}'')\epsilon^{-1}_{(\mathrm{RPA})}(\boldsymbol{r}'', \boldsymbol{r}'). \tag{4.2}$$

Thus, given a (necessarily approximated) expression for $\epsilon^{-1}_{(\mathrm{RPA})}$, one can in principle calculate all response functions. We focus on two RPA models for the inverse dielectric function of insulators: the CDRB model [12] and that given by LL [11]. In these models, $\epsilon^{-1}_{(\mathrm{RPA})}(\boldsymbol{r}, \boldsymbol{r}')$ is taken as a function of $|\boldsymbol{r} - \boldsymbol{r}'|$ only. LF effects are nevertheless reintroduced by means of a local ansatz: in the reciprocal space, the inverse dielectric function is written as a function of the wavevector modulus $q = |\boldsymbol{q}|$ and the local density $n(\boldsymbol{r})$. $W(\boldsymbol{r}, \boldsymbol{r}')$ can then be written,

following the ansatz of Hybertsen and Louie [13], as

$$W(\boldsymbol{r},\boldsymbol{r}') = \frac{1}{2(2\pi)^3}\left[\int v(\boldsymbol{q})\epsilon^{-1}_{(\mathrm{RPA})}(|\boldsymbol{q}|, n(\boldsymbol{r}))\mathrm{e}^{\mathrm{i}\boldsymbol{q}\cdot(\boldsymbol{r}-\boldsymbol{r}')}\,\mathrm{d}\boldsymbol{q} + \int v(\boldsymbol{q})\epsilon^{-1}_{(\mathrm{RPA})}(|\boldsymbol{q}|, n(\boldsymbol{r}'))\mathrm{e}^{\mathrm{i}\boldsymbol{q}\cdot(\boldsymbol{r}-\boldsymbol{r}')}\,\mathrm{d}\boldsymbol{q}\right]. \tag{4.3}$$

The inverse *macroscopic* dielectric function $\tilde{\epsilon}^{-1}_{(\mathrm{RPA})}(\boldsymbol{q})$ is thus equal to

$$\tilde{\epsilon}^{-1}_{(\mathrm{RPA})}(\boldsymbol{q}) = \frac{1}{\Omega}\int_{\Omega}\mathrm{d}\boldsymbol{r}\,\epsilon^{-1}_{(\mathrm{RPA})}(\boldsymbol{q}, n(\boldsymbol{r})), \tag{4.4}$$

(where Ω is the volume of the unit cell) and its limit at small values of $\boldsymbol{q}$ is the inverse of the optical dielectric constant ϵ_∞. In the opposite limit $q \to \infty$, any RPA dielectric function must behave as the Lindhardt dielectric function [12]. These requirements give two constraints that every model for the *microscopic* dielectric functions must fulfil: one can show for example, by computing the response to a periodic Coulomb potential with a neutralizing background of charge, that it is necessary that $\epsilon^{-1}(\boldsymbol{q}, n(\boldsymbol{r})) \to 1/\epsilon_\infty$ in the limit $q \to 0$, whatever $\boldsymbol{r}$, in order that no divergence of the total potential occurs. The CDRB dielectric function is defined as

$$\epsilon_{\mathrm{CDRB}}(q, n(\boldsymbol{r})) = 1 + \frac{1}{A[n(\boldsymbol{r})] + B[n(\boldsymbol{r})]q^2 + C[n(\boldsymbol{r})]q^4}, \tag{4.5}$$

with $A[n(\boldsymbol{r})] = 1/(\epsilon_\infty - 1)$, $B[n(\boldsymbol{r})] = 1/q^2_{\mathrm{TF}}[n(\boldsymbol{r})]$, and $C[n(\boldsymbol{r})] = 3/(4q^2_{\mathrm{TF}}[n(\boldsymbol{r})]k^2_{\mathrm{F}}[n(\boldsymbol{r})])$.

The LL model has a more complex expression:

$$\epsilon_{\mathrm{LL}}(q, n(\boldsymbol{r})) = 1 + \frac{1}{k_{\mathrm{F}}\pi}\left[\frac{1}{Q^2} - \frac{\lambda}{2Q^2}\left[\arctan\frac{2Q+Q^2}{\lambda} + \arctan\frac{2Q-Q^2}{\lambda}\right] + \left[\frac{\lambda^2}{8Q^5} + \frac{1}{2Q^3} - \frac{1}{8Q}\right]\ln\left(\frac{\lambda^2 + (2Q+Q^2)^2}{\lambda^2 + (2Q-Q^2)^2}\right)\right]. \tag{4.6}$$

In those expressions, $Q = q/k_{\mathrm{F}}[n(\boldsymbol{r})]$ and $\lambda = 16\pi n(\boldsymbol{r})/(k^4_{\mathrm{F}}[n(\boldsymbol{r})](\epsilon_{\infty-1}))$. LF effects are introduced through the dependence of the Fermi wavevector k_{F}, the Thomas–Fermi wavevector q_{TF}, and λ on the local density[4].

The two models fulfil the requirements for the dielectric function at small and large wavevectors. They contain two parameters: the optical dielectric constant and the local electron ground-state density. For the semiconductors and insulators under study, we adopt the experimental value of the optical dielectric constant ϵ_∞ [24] and the local density is taken from the DFT-LDA calculation of the unperturbed ground state ($n(\boldsymbol{r}) = n_0(\boldsymbol{r})$).

4.2. Testing and improvement of the RPA models

Within the RPA, we compare the potentials induced by the Gaussian perturbation (equation (2.5)) that are computed within the direct method or by using the CDRB (equation (4.5)) and the LL (equation (4.6)) model dielectric functions. We quantify the quality of those models by means of the coefficients $\Theta^{(\mathrm{LL})}_V$ and $\Theta^{(\mathrm{CDRB})}_V$ (equation (2.6)). The perturbation is chosen at various sites $\boldsymbol{r}_0$, in order to obtain a clear picture of LF effects. Either it is centred on the atom A (and accordingly labelled in tables 1 and 3) or it is located along the line connecting atoms A and B and labelled 'x A–B'.

The LL model appears to be slightly superior to the CDRB one for Si, while their overall precisions are nearly identical for $SrTiO_3$ and MgO. Figure 5 shows in detail the behaviour of $V^{(\mathrm{CDRB})}_{\mathrm{ind}}$ along the Mg–O bond in magnesium oxide, when the perturbation is located midway

[4] $k_{\mathrm{F}}[n(\boldsymbol{r})] = (3\pi^2)^{2/3}n(\boldsymbol{r})^{2/3}$ and $q_{\mathrm{TF}}[n(\boldsymbol{r})] = (4k_{\mathrm{F}}(n(\boldsymbol{r}))/\pi a_0)^{1/2}$, where a_0 is the Bohr radius.

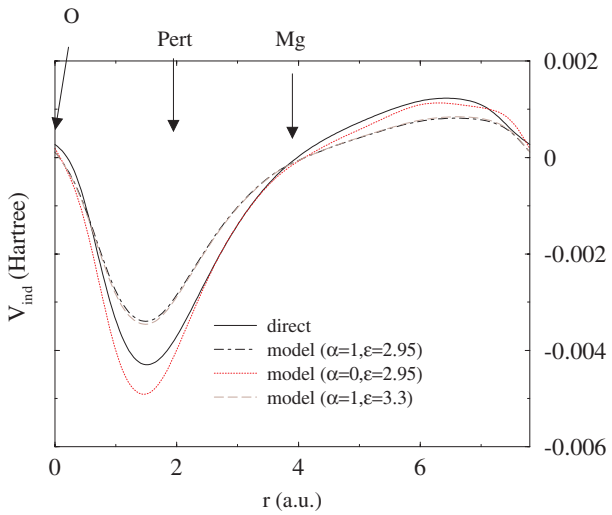

Figure 5. The induced potential $V_{\rm ind}^{\rm RPA}$ computed within the RPA in response to a Gaussian potential localized between O and Mg in MgO. The potential computed via the direct method (direct) is compared to those obtained through the use of the CDRB model dielectric function (equation (4.5)) by adopting different values for α and ϵ_∞ (see the text). The positions of the perturbation (Pert) and of the Mg and O atoms are shown by an arrow.

Table 1. Values of $\Theta_V^{\rm (LL)}$ and $\Theta_V^{\rm (CDRB)}$ in Si for different perturbation sites $\boldsymbol{r}_0$. The second line gives the ground-state density at the point where the perturbation is centred. The site −1 Si–Si is interstitial.

$\boldsymbol{r}_0$	0.5 Si–Si	−1 Si–Si	0.25 Si–Si
$n(\boldsymbol{r}_0)$ (au^{-3})	0.086	0.0033	0.065
$\Theta_V^{\rm (CDRB)}$	0.26	0.38	0.36
$\Theta_V^{\rm (LL)}$	0.16	0.23	0.24

Table 2. Values of $\Theta_V^{\rm (LL)}$ and $\Theta_V^{\rm (CDRB)}$ in MgO for different perturbation sites. The notation is the same as in table 1.

$\boldsymbol{r}_0$	0.25 O–Mg	0.5 O–Mg	Mg	O
$n(\boldsymbol{r}_0)$ (au^{-3})	0.44	0.05	0.014	0.25
$\Theta_V^{\rm (CDRB)}$	0.40	0.24	0.34	0.50
$\Theta_V^{\rm (LL)}$	0.42	0.15	0.40	0.52

between O and Mg. The largest failure is happening close to the perturbation site, where the model underestimates the response. In addition, the oscillations of $n_{\rm ind}(\boldsymbol{r}_0)$ in the vicinity of the nuclei (O, Sr, and Ti) are not reproduced.

In order to improve such models while keeping the same simplified treatment of LF effects, we consider the class of microscopic dielectric functions of the form $\epsilon(q, n(\boldsymbol{r}))$ given in equation (4.5). The CDRB model corresponds to the particular choice $A = 1/(\epsilon_\infty - 1)$, $B[n(\boldsymbol{r})] = 1/q_{\rm TF}^2[n(\boldsymbol{r})]$, and $C[n(\boldsymbol{r})] = 3/(4q_{\rm TF}^2[n(\boldsymbol{r})]k_{\rm F}^2[n(\boldsymbol{r})])$.

Firstly, there is no constraint about the actual form of $B[n(\boldsymbol{r})]$. Cappellini *et al* [12] argued that it can be determined from a fit of the macroscopic dielectric function that can be

Table 3. Values of $\Theta_V^{(\mathrm{LL})}$ and $\Theta_V^{(\mathrm{CDRB})}$ in $SrTiO_3$ for different perturbation sites.

$\boldsymbol{r}_0$	Ti	Sr	O	0.5 O–Ti	0.5 Sr–Ti	0.25 O–Ti	0.75 O–Ti
$n(\boldsymbol{r}_0)$ (au^{-3})	0.24	0.12	0.29	0.11	0.013	0.52	0.94
$\Theta_V^{(\mathrm{CDRB})}$	0.25	0.17	0.44	0.22	0.24	0.28	0.26
$\Theta_V^{(\mathrm{LL})}$	0.30	0.10	0.47	0.20	0.15	0.30	0.29

Table 4. Values of $\Theta_{V^{\mathrm{RPA}}}^{(\alpha)}$ in MgO, obtained for different sites $\boldsymbol{r}_0$, though the two screening models given in equation (4.5), by using different values for the B-coefficient (see the text).

$\boldsymbol{r}_0$	0.25 O–Mg	0.5 O–Mg	Mg	O
$n(\boldsymbol{r}_0)$ (au^{-3})	0.44	0.05	0.014	0.25
$\Theta_V^{(\alpha=1)}$	0.40	0.24	0.34	0.5
$\Theta_V^{(\alpha=0)}$	0.23	0.14	0.48	0.3

Table 5. Values of $\Theta_{V^{\mathrm{RPA}}}^{(\alpha)}$ in $SrTiO_3$, obtained for different sites $\boldsymbol{r}_0$, through the two screening models given in equation (4.5), by using different values for the B-coefficient (see the text).

$\boldsymbol{r}_0$	0.5 O–Ti	0.5 Sr–Ti	0.25 O–Ti	0.75 O–Ti	Ti	O
$n(\boldsymbol{r}_0)$ (au^{-3})	0.11	0.013	0.52	0.94	0.24	0.29
$\Theta_V^{(\alpha=1)}$	0.22	0.24	0.28	0.26	0.25	0.44
$\Theta_V^{(\alpha=0)}$	0.41	0.20	0.19	0.14	0.125	0.25

obtained from first principles, but only the microscopic ϵ is of interest here, and the relation between the latter two (equation (4.4)) cannot be straightforwardly inverted in inhomogeneous systems. Therefore, we adopt the functional form $B[n(\boldsymbol{r})] = \alpha/q_{\mathrm{TF}}^2[n(\boldsymbol{r})]$ and allow α to vary (in practice, variations in the range $-1 \leqslant \alpha \leqslant 2$ are sufficient for our purposes). Considering several sites for the perturbation, we compute the coefficient $\Theta_V^{(\alpha)}$, which quantifies the success of the model at reproducing the induced potential as a function of the α-parameter. The results are compared in tables 4 and 5.

Secondly, the choice of a particular value for ϵ_∞ should in principle rely on an independent RPA calculation. For practical reasons, we adopt here the experimental ϵ_∞ [24], since the RPA is expected to yield a value pretty close to the experimental one [2]. In order to check the sensitivity of the computed induced potential to the actual ϵ_∞, we evaluate V_{ind} in MgO by using the model 4.5 with $\alpha = 0$ and $\epsilon_\infty = 3.3$, which represents a limiting case, since $\epsilon_\infty = 3.03$ in the LDA as computed by Shirley [25]. The quality coefficients Θ_V that are listed in the tables change by a few per cent, and the induced potentials that are computed by using $\epsilon_\infty = 3.3$ or 2.95 hardly differ (see figure 5 for an example).

In MgO and $SrTiO_3$, the minimum of $\Theta_V^{(\alpha)}$ is found for $\alpha \in [-0.5, 0.5]$, whatever the perturbation site, and the value $\alpha = 0$ is a good compromise for reproducing the overall features of the induced potential. In addition, as shown in table 4, a smaller value of $\Theta_V^{(\alpha=0)}$ results for most of the perturbation sites. As an illustration, we plot in figure 5 the induced potential for $\alpha = 0$, which is clearly improved with respect to the $\alpha = 1$ case, in full accordance with table 4. For silicon, the minimum is shallower and an optimized value $\alpha = 1$ is deduced.

By adopting $\epsilon(q, n(\boldsymbol{r}))$ (equation (4.5)), the macroscopic dielectric function $\tilde{\epsilon}(\boldsymbol{q})$ can be estimated from equation (4.4). Interestingly, in the case of MgO and $SrTiO_3$, we find the

macroscopic dielectric function to be well fitted by a function of the type 4.5 with $\alpha = 1$ and the average density replacing $n(\boldsymbol{r})$, in agreement with what was found by Cappellini *et al* for silicon [12]. Therefore, if one aims to mimic simply the *macroscopic* static dielectric function without worrying too much about the induced potential, the CDRB model ($\alpha = 1$) with the mean density provides a good fit.

4.3. Discussion

Both CDRB and LL models describe the on-site response in different crystals fairly well for various perturbation sites. In contrast, the rather large values of the quality factors $\Theta_V^{(\mathrm{LL})}$ and $\Theta_V^{(\mathrm{CDRB})}$, especially for ionic materials such as MgO and $SrTiO_3$ where some errors may be upwards of 50% (see tables 1–5), mainly come from the failure of the CDRB and the LL models to reproduce the medium-range oscillations of the induced density. Indeed, the latter ones originate mainly from the phases of the eigenstates at the VB maximum and CB minimum, which are completely discarded in any formulation of LF effects that is based upon the local density.

In general, the CDRB model (modified or not) can describe with a good accuracy the short-range induced potential created by a localized perturbation. However, for some positions of the perturbation (at the Mg site in MgO, midway between the O and the Ti in $SrTiO_3$), the results are not satisfactory even when one allows α to vary (see table 4). As was said before, the actual value of ϵ_∞ has a marginal influence and the use of an optical dielectric constant that is computed within the RPA for each material, although possible in practice and logically more consistent, cannot in any case improve the quality of the induced potentials that are obtained from the model dielectric functions. At those sites, the oscillations of the induced potential are as intense as the potential depletion near the perturbation site (partly because the local density on the perturbation site is very weak), and the weakness of local-density-based models is thus particularly evident. In the next section, we come back to the representation of the non-interacting polarizability χ_0 in terms of the Kohn–Sham wavefunctions, which seems to be unavoidable whenever the medium-range oscillations of the induced density have to be reproduced, and we propose a practical way to lighten the computational burden of its numerical calculation.

5. *Ab initio* calculation of the polarizability

5.1. Method

We restrict ourselves to the calculation of the non-interacting static polarizability χ_0 because it is a key quantity from which one can calculate the inverse dielectric function in the RPA or beyond (including the kernel K_{xc} in the LDA), i.e. all the screening properties of the system (see section 2). For diamagnetic systems, χ_0 can be written as

$$\chi_0(\boldsymbol{r}, \boldsymbol{r}') = 4 \sum_{i.j} \frac{f_i(1 - f_j)}{\epsilon_j - \epsilon_i} [\phi_i^*(\boldsymbol{r})\phi_j(\boldsymbol{r})\phi_j^*(\boldsymbol{r}')\phi_i(\boldsymbol{r}')] \tag{5.1}$$

where ϕ_i, ϵ_i, and f_i are the Kohn–Sham wavefunctions, eigenvalues, and occupation factors, respectively. At zero temperature, the summation runs over the occupied (i) and the empty states (j). We note that $\chi_0(\boldsymbol{r}, \boldsymbol{r}')$ is invariant with respect to the exchange of $\boldsymbol{r}$ and $\boldsymbol{r}'$. Once χ_0 is known, the density $n_{\mathrm{ind}}^{(\mathrm{NSC})}$ induced by any V_{pert} can be computed through the relations (2.2) and (2.4).

It can be easily realized that the contribution of each single state (either i or j) to χ_0 in equation (5.1) roughly decreases inversely to its energy distance from the Fermi level and is

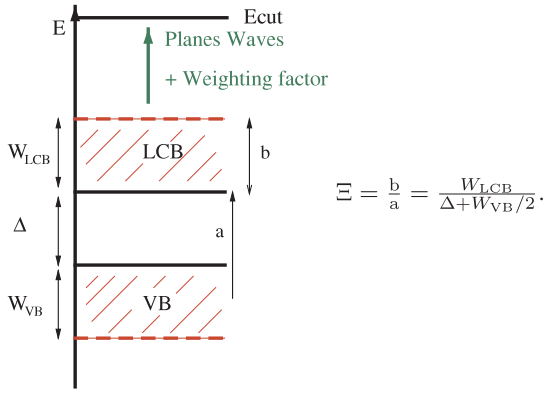

Figure 6. The schematic energy diagram. W_{LCB} and W_{VB} are the bandwidths for the lower conduction band (LCB) and the VB. LCB refers to the band of conduction states computed in the DFT-LDA. Δ is the minimum *gap* as given by a DFT-LDA calculation.

modulated by the $i-j$ overlap. The sum over CB states converges slowly and, as recognized in [2], it is necessary to include a large number of CB states to compute χ_0 accurately. Nevertheless, as shown by Steinbeck *et al* [6], beyond a given energy, the CB states can be replaced by plane waves (PWs) in equation (5.1). The PW contribution to equation (5.1) can be analytically evaluated, thus lightening the computational burden. This approximation yields much better results for Si than for more ionic semiconductors such as GaN. Moreover, the same authors have shown that the results are not sensitive to the use of symmetrized PWs, which is in principle required. In the same spirit as [6], we compute χ_0 from equation (5.1) by including N_{e} Kohn–Sham states in the j-summation over CB, up to an energy that lies W_{LCB} above the CB minimum (figure 6). The remaining states, up to the cut-off energy E_{cut}, are taken as PWs. The energy of a $(\boldsymbol{k}+\boldsymbol{G})$ PW is written as $E_{\mathrm{inf}}+|\boldsymbol{G}+\boldsymbol{k}|^2/2$, where E_{inf} is the extrapolated bottom of the PW band that can be determined by the requirement of conservation of the number of states:

$$\int_{E_{\mathrm{inf}}}^{E_{\mathrm{cut}}} n_{\mathrm{PW}}(E)\,\mathrm{d}E = \frac{N_{\mathrm{e}}}{\Omega} \tag{5.2}$$

(where $n_{\mathrm{PW}}(E)$ is the PW density of states and Ω the volume of the unit cell). According to equation (5.2), the lowest-energy PW introduced in the sum (5.1) is the $N_{\mathrm{e}}+1$th CB state on the energy scale. In the following, we call the PW and Kohn–Sham CB state contributions to the polarizability χ_{PW} and χ_{LCB}, respectively. The simple assumption $\chi_0=\chi_{\mathrm{LCB}}+\chi_{\mathrm{PW}}$ gives contrasting results for ionic compounds [6]. For this reason, we use the following ansatz:

$$\chi_\beta(\boldsymbol{r},\boldsymbol{r}') = \chi_{\mathrm{LCB}}(\boldsymbol{r},\boldsymbol{r}') + \mathrm{e}^{-\beta[n(\boldsymbol{r})+n(\boldsymbol{r}')]}\chi_{\mathrm{PW}}(\boldsymbol{r},\boldsymbol{r}'). \tag{5.3}$$

The weighting factor $\mathrm{e}^{-\beta[n(\boldsymbol{r})+n(\boldsymbol{r}')]}$ modulates the PW contribution in direct space, while preserving the symmetry of $\chi_0(\boldsymbol{r},\boldsymbol{r}')$ with respect to interchange of $\boldsymbol{r}$ and $\boldsymbol{r}'$. Its use can be qualitatively justified as follows. Unlike PWs, the Kohn–Sham CB state density is not uniform in space. In particular, taking into account the closure relation and the fact that the ground-state density $n_0(\boldsymbol{r})$ is built from VB states, one can easily realize that CB states are preferentially located away from the nuclei, in regions in which $n_0(\boldsymbol{r})$ is rather low. Thus, replacing high-energy CB states with PWs in equation (5.1) leads to an error in those regions that we partially correct by introducing the energy-independent weighting factor $\mathrm{e}^{-\beta[n(\boldsymbol{r})+n(\boldsymbol{r}')]}$. As shown in the following section, such an approximation clearly improves the quality of the

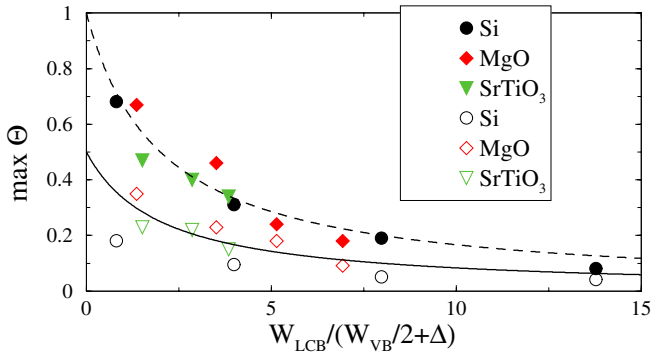

Figure 7. $\max \Theta^{(\chi_{\mathrm{LCB}})}$ (filled symbols) and $\max \Theta^{(\chi_\beta)}$ (empty symbols) as a function of $W_{\mathrm{LCB}}/(W_{\mathrm{VB}}/2 + \Delta)$ in the cases of Si, MgO, and $SrTiO_3$.

computed χ_0 for both covalent and ionic crystals, provided that the β-factor is chosen in a reasonable range.

One can easily see that the larger the number N_e of CB states explicitly included in the sum (5.1), the better the approximation (5.3). It is also to be noted that a remarkable computational speed-up may in principle be achieved by replacing the sum on high-energy CB states with the weighted PW contribution, since χ_{PW} in equation (5.3) can be rewritten in an analytical form well suited to a fast calculation.

In order to analyse the performances of this computational scheme for χ_0 in materials with various degrees of ionic and covalent bonding, we introduce the coefficient $\Xi = W_{\mathrm{LCB}}/(\Delta + W_{\mathrm{VB}}/2)$. It is the ratio of the lower CB width W_{LCB} (see caption of figure 6) to the difference between the CB minimum and the centre of the VB ($\Delta + W_{\mathrm{VB}}/2$). Ξ is a universal quantity which takes into account the number of CB states included in equation (5.1) normalized with respect to the main features of the electronic structure such as the valence bandwidth and the fundamental gap. In the limit of very large value of Ξ, the exact result for χ_0 is recovered. For Ξ close to one, we find that approximation (5.3) is superior to other computational schemes used previously.

5.2. *Results and discussion*

In a first step, for the three materials Si, MgO, and $SrTiO_3$, we keep in the summation 3.1 only the CB states obtained in the LDA (i.e. no PWs at all) thus obtaining χ_{LCB}. Then, by placing the Gaussian perturbation V_{pert} at various sites, we compute the induced density as $\chi_{\mathrm{LCB}}[V_{\mathrm{ind}}^{(\mathrm{LDA})} + V_{\mathrm{pert}}]$ and compare it to that extracted by the direct method through the quality coefficients $\Theta_n^{(\chi_{\mathrm{LCB}})}$. In silicon we choose the sites 0.5 Si–Si, 0.25 Si–Si, and -1 Si–Si; in MgO the sites Mg, O, 0.5 O–Mg, and 0.25 O–Mg; in $SrTiO_3$ the sites 0.25 O–Ti, 0.5 O–Ti, 0.75 O–Ti, and 0.5 Sr–Ti.

In figure 7, the maximal values of $\Theta_n^{(\chi_{\mathrm{LCB}})}$ among all sites are plotted as a function of Ξ. As expected, $\max \Theta$ decreases as Ξ gets larger, i.e. when more Kohn–Sham CB states are included. It is worth noting that the points corresponding to the different crystals fall on the same curve. Its universality shows that Ξ is the relevant parameter for characterizing the convergence of the *ab initio* calculation of χ_0, whatever the VB–CB gap width and the specific electronic density of states.

In a second step, we repeat the same procedure, but we complement the summation with

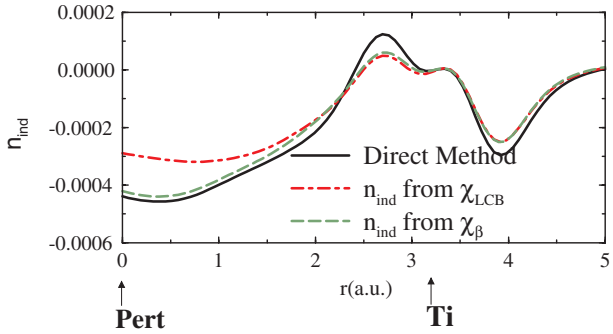

Figure 8. The induced density $n_{\rm ind}$ (in au^{-3}) for a Gaussian repulsive perturbation centred halfway between Sr and Ti (labelled 'Pert'). $n_{\rm ind}^{\rm direct}$ is compared to induced densities computed by means of $\chi_{\rm LCB}$ and χ_β, with $N_{\rm e} = 40$.

weighted PWs (equation (5.3)). We thus obtain χ_β, the quality of which is estimated through $\Theta_n^{(\chi_\beta)}$. Then, similarly to the case for $\chi_{\rm LCB}$, we define max $\Theta_n^{(\chi_\beta)}$ as the maximum of $\Theta_n^{(\chi_\beta)}$ among all perturbation sites, for Si, MgO, and $SrTiO_3$ and different Ξ. max $\Theta^{(\chi_\beta)}$ obviously depends on the weighting parameter β. Therefore, we determine the optimal weighting parameter which minimizes max Θ_β for all materials and in the whole range of Ξ. This yields the value $\beta \simeq 1$ au^3. It must be noted that the optimal weighting is rather independent of the actual location of the perturbation and the precise value of Ξ—related to the number of CB states included—varying at most by $\simeq$3% around $\beta = 1$. This suggests that the weighting procedure (equation (5.3)) captures the essential features of the contribution of high-energy CB states to the polarizability, for crystals over a wide range of iono-covalent bonding. From a practical point of view, the introduction of the PW weighting leads to an improvement on max Θ by a factor 2 (in the cases of MgO and $SrTiO_3$) or even 3 (for silicon). In agreement with what was obtained by Steinbeck *et al* for GaN [6], we find that the inclusion of PWs with no weighting (i.e. $\beta = 0$ in equation (5.3)) does not improve Θ in the cases of MgO and $SrTiO_3$.

To show how the weighting procedure (equation (5.3)) works, we compare in figure 8 the induced densities computed by the direct method, from $\chi_{\rm LCB}$ and from χ_β plotted along a Sr–Ti bond in $SrTiO_3$ when a perturbing Gaussian potential is located halfway between the atoms. We see that the induced density close to the Ti atom is well accounted for through the use of $\chi_{\rm LCB}$. However, the response is underestimated in the low-density region close to the perturbation. The inclusion of weighted PWs clearly improves $n_{\rm ind}$ in the interstitial region, where the contribution of the lower CB states is very weak and the absolute induced density accordingly underestimated, without affecting it much elsewhere.

Since the optimum value of the weighting parameter β and the curves in figure 7 are rather insensitive to the crystal under study, a systematic procedure for optimizing the computational set-up of the non-interacting polarizability χ_0 can be established. Given a required precision max Θ on $n_{\rm ind}(\boldsymbol{r})$, the full curve in figure 7 yields $W_{\rm LCB}/(\Delta + W_{\rm VB}/2)$ from which, knowing the electronic structure of the compound (i.e. the VB width $W_{\rm VB}$ and the fundamental gap Δ), the number $N_{\rm e}$ of CB states to be explicitly calculated can be extracted. PWs are then added up to the cut-off energy $E_{\rm cut}$ with the optimal weighting factor $e^{-[n(r)+n(r')]}$.

We end with a last remark regarding the computational speed-up that can be obtained by using weighted PWs in the calculation of the static polarizability (equation (5.3)), at a given level of precision as indicated by max Θ in figure 7. If one needs to reach a precision of, let

us say, about 30% on the induced density in $SrTiO_3$, the conduction bandwidth W_{LCB} to be considered is about a half of that needed without adding PWs to obtain the same precision. The resulting speed-up turns out to be by a factor bigger than 3, since the computation of the PW contribution χ_{PW} to the polarizability is in practice very inexpensive with respect to that of χ_{LCB}. For larger-size systems, for which the computation of CB states is expensive, the speed-up that can be obtained by using equation (5.3) may rise up to a factor ten.

6. Conclusions

In this paper, we have discussed some fundamental and practical issues concerning screening properties in semiconductors and insulators. We have chosen the three cubic crystals Si, $SrTiO_3$, and MgO, whose bonding spans a wide range of ionicity strengths and optical dielectric constants.

We have carried out a direct-space numerical calculation of the density induced by a localized, time-independent repulsive perturbation, in the framework of the DFT. The short- and medium-range features of the screening have been discussed, which include a depletion of electrons close to the perturbation and density oscillations with atomic-like features in the vicinity of the nuclei.

We have addressed the question of how LFs can be mimicked by simplified models of the microscopic static dielectric function that use the unperturbed ground-state local density as the basic variable. We have shown that the short-range screening can be qualitatively well reproduced, and we suggest a simple improvement for their description within the same class of models. On the other hand, we have found that the oscillatory behaviour of the induced density in the real space cannot be accounted for.

Finally, we propose a simplified method for performing the *ab initio* computation of the one-electron static polarizability, in which the contribution of high-energy CB states is replaced by a weighted sum over PWs. Such a method lightens the numerical calculational burden considerably and may thus open the way to the computation of static response functions of large systems.

Acknowledgments

We acknowledge fruitful discussions with Lucia Reining and Rodolfo Del Sole. We are grateful to IDRIS for the allocation of computer resources under project no 14089.

References

[1] Pines D and Nozières P 1966 *The Theory of Quantum Liquids I* (Menlo Park, CA: Benjamin)
[2] Hybertsen M S and Louie S G 1987 *Phys. Rev.* B **35** 5585
[3] Albaret T, Finocchi F and Noguera C 1999 *Faraday Discuss.* **114** 285
[4] Godby R W, Schlüter M and Sham L J 1988 *Phys. Rev.* B **37** 10 159
[5] Hybertsen M S and Louie S G 1986 *Phys. Rev.* B **34** 5390
[6] Steinbeck L, Rubio A, Reining L, Torrent M, White I D and Godby R W 2000 *Comput. Phys. Commun.* **125** 105
[7] Gygi F and Baldereschi A 1989 *Phys. Rev. Lett.* **62** 2160
[8] Zhu X and Louie S G 1991 *Phys. Rev.* B **43** 14 142
[9] Bechstedt F, Del Sole R, Cappellini G and Reining L 1992 *Solid State Commun.* **84** 765
[10] Penn D R 1962 *Phys. Rev.* **128** 2093
[11] Levine Z H and Louie S G 1982 *Phys. Rev.* B **25** 6310
[12] Cappellini G, Del Sole R, Reining L and Bechstedt F 1993 *Phys. Rev.* B **47** 9892
[13] Hybertsen M S and Louie S G 1988 *Phys. Rev.* B **37** 2733
[14] Palummo M, Del Sole R, Reining L, Bechstedt F and Cappellini G 1995 *Solid State Commun.* **95** 393

[15] Cappellini G, Bouette-Russo S, Amadon B, Noguera C and Finocchi F 2000 *J. Phys.: Condens. Matter* **12** 3671
[16] Abrikosov A A, Gorkov L P and Dzyaloshinski I E 1963 *Methods of Quantum Field Theory in Statistical Physics* (Englewood Cliffs, NJ: Prentice-Hall)
[17] Ceperley D M and Alder B J 1980 *Phys. Rev. Lett.* **45** 566
[18] Perdew J P and Zunger A 1981 *Phys. Rev.* B **23** 5048
[19] See e.g. Aryasetiawan F and Gunnarsson O 1998 *Rep. Prog. Phys.* **61** 237
[20] Baroni S, De Gironcoli S, Dal Corso A and Giannozzi P 2001 *Rev. Mod. Phys.* **73** 515
[21] Troullier N and Martins J L 1991 *Phys. Rev.* B **43** 1993
[22] Hybertsen M S and Louie S G 1987 *Phys. Rev.* B **35** 5602
[23] Resta R and Baldereschi A 1981 *Phys. Rev.* B **23** 6615
[24] We use the experimental values $\epsilon_\infty(\mathrm{Si}) = 11.7$, $\epsilon_\infty(\mathrm{SrTiO_3}) = 5.82$ from
Dore P, Paolone A and Trippetti R 1996 *J. Appl. Phys.* **80** 5271
and $\epsilon_\infty(\mathrm{MgO}) = 2.95$ from
Whited R C, Flaten C J and Walker W C 1973 *Solid State Commun.* **13** 1903
[25] Shirley E 1998 *Phys. Rev.* B **58** 9579